Laser Cavity-Soliton Micro-Combs

Hualong Bao[1], Andrew Cooper[1], Maxwell Rowley[1], Luigi Di Lauro[1], Juan Sebastian Totero Gongora[1], Sai T. Chu[2], Brent E. Little[3], Gian-Luca Oppo[4], Roberto Morandotti[5,6,7], David J. Moss[8], Benjamin Wetzel[1], Marco Peccianti[1] and Alessia Pasquazi[1*]

[1]*Emergent Photonics (Epic) Lab, Dept. of Physics and Astronomy, University of Sussex, BN1 9QH, UK*
[2]*Department of Physics, City University of Hong Kong, Tat Chee Avenue, Hong Kong, China SAR*
[3]*State Key Laboratory of Transient Optics and Photonics, Xi'an Institute of Optics and Precision Mechanics, CAS, Xi'an, China*
[4]*SUPA, Department of Physics, University of Strathclyde, Glasgow, United Kingdom*
[5]*INRS-EMT, 1650 Boulevard Lionel-Boulet, Varennes, Québec, Canada J3X 1S2*
[6]*Institute of Fundamental and Frontier Sciences, University of Electronic Science and Technology of China, Chengdu 610054, Sichuan, China*
[7]*ITMO University, St. Petersburg 199034, Russia*
[8]*Centre for Microphotonics, Swinburne University of Technology, Hawthorn, VIC 3122, Australia*

**Corresponding author: a.pasquazi@sussex.ac.uk*

Micro-cavity based frequency combs, or 'micro-combs' [1,2], have enabled many fundamental breakthroughs [3-21] through the discovery of temporal cavity-solitons. These self-localised waves, described by the Lugiato-Lefever equation [22], are sustained by a background of radiation usually containing 95% of the power [23]. Simple methods for their efficient generation and control are currently being investigated to finally establish micro-combs as out-of-the-lab tools [24].

Here, we demonstrate *micro-comb laser* cavity-solitons. Laser cavity-solitons are intrinsically background free and have underpinned key breakthroughs in semiconductor lasers [22,25-28]. By merging their properties with the physics of multi-mode systems [29], we provide a new paradigm for soliton generation and control in micro-cavities. We demonstrate 50 nm wide bright soliton combs induced at average powers more than *one order of magnitude* lower than the Lugiato-Lefever soliton power threshold [22], measuring a mode efficiency of 75% versus the theoretical limit of 5% for bright Lugiato-Lefever solitons [23]. Finally, we can tune the repetition-rate by well over a megahertz without any active feedback.

Optical frequency combs based on micro-cavity resonators, also called 'micro-combs', offer the promise of achieving the full capability of their bulk counterparts, yet in an integrated footprint [1, 2]. They have enabled major breakthroughs in spectroscopy [3,4], communications [5,6] microwave photonics [7], frequency synthesis [8], optical ranging [9,10], quantum sources [11, 12], metrology [13,14] and astrocombs [15,16].

Of particular importance has been the discovery of temporal cavity-solitons in micro-cavities [17-21]. Temporal cavity-solitons [2,17-23] are an important example of dissipative solitons – self-confined waves balancing dispersion with the nonlinear phase-shift in lossy systems [30]. Practical applications of these pulses for micro-combs, however, still face significant challenges. In particular, they achieve a limited *mode efficiency*, defined as the fraction of optical power residing in the comb modes other than the most powerful one. Solitons in micro-cavities exist as localised states upon a background, usually a continuous-wave (CW) [2,17-23], which results in a dominant mode in the comb spectrum. In this configuration, described by the well-known Lugiato-Lefever equation, bright solitons have a mode efficiency

Accepted author manuscript of the following peer-reviewed research article: Bao, H., Cooper, A., Rowley, M., Di Lauro, L., Totero Gongora, J. S., Chu, S. T., ... Pasquazi, A. (2019). Laser cavity-soliton microcombs. Nature Photonics. https://doi.org/10.1038/s41566-019-0379-5

theoretically bounded to 5% [23], limiting the efficiency of state-of-the-art micro-combs based on this operating principle [2,23-24,31].

Furthermore, controlling their fundamental parameters, such as repetition-rate, has posed a challenge. Currently, tuning their repetition-rate requires either complex methods involving fast detection, microwave signal processing and fast cavity actuation, or novel approaches such as pulsed [16,32] or counter-propagating [33] pumping, or heterodyning with coupled micro-resonators [34]. Finding a solution to these fundamental issues has attracted significant effort [24, 31].

Here, we demonstrate a distinct class of solitary pulses in micro-combs – temporal ***laser*** cavity-solitons – that directly addresses these challenges. Laser cavity-solitons [22,25-28] have been largely studied in spatial configurations such as semiconductor lasers [25], where they enabled breakthroughs such as all-optical reconfigurable memories [26]. More recently, they have been observed in both temporal [28] and spatio-temporal [35] contexts. They are fundamentally different to externally driven cavity-solitons, which are sustained by the energy of the pumping background. Laser cavity-solitons, in contrast, receive energy directly from the gain of the lasing medium. As result, they exist without any background light and are intrinsically the most energy efficient class of cavity-solitons.

By nesting a Kerr micro-resonator in a fibre loop with gain, we harvest the intrinsic capability of laser cavity-solitons, demonstrating that they can be used to achieve highly efficient, broadband micro-comb generation. We excite bright solitons having a bandwidth of more than 50 nm, using average powers less than ***6% of the threshold*** for Lugiato-Lefever solitons in an equivalent resonator. Our background-free solitons have a *mode efficiency* of 75%, with a theoretical maximum predicted to be 96%. Furthermore, by exploring the properties of multi-mode systems, recently investigated for spatio-temporal mode-locking [29] and spatial beam self-cleaning [36], we show that the repetition-rate of our pulses can be adjusted by reconfiguring simple parameters such as the laser cavity-length. Without the use of active control, we succeed in modifying their repetition-rate by more than a megahertz.

The principle of operation is shown in Fig. 1a. A nonlinear micro-cavity (cavity 'a') is embedded within a longer amplifying fibre cavity (cavity 'b'). The pulse propagating in the fibre loop, spectrally limited by the laser-gain bandwidth, sustains in the micro-cavity the existence of a pulse which is broadened by the Kerr nonlinearity over the gain bandwidth [25,37]. This architecture is inspired by the concept of a filter-driven four-wave mixing laser [38]. Our present analysis allows us to define the solitary state existence and understand the nature of previous observations [2,38,39]. In particular, we show that the relative position of the oscillating modes within the micro-cavity resonances is critical to realise this new class of broadband solitary pulses.

Temporal cavity-solitons can be effectively modelled using mean-field approaches, such as the Lugiato-Lefever equation [17], where the field in the micro-cavity is described as a pulse propagating in time, along with a spatial coordinate periodically looped within the micro-resonator length. Here, we build a set of multi-component (or 'vectorial') laser mean-field equations [29,36] by coupling together the micro-cavity field with the main-cavity 'super-mode' fields. (Supplementary/Methods). A super-mode is an optical radiation formed by a set of equally-spaced modes of the main-cavity, whose relative spacing (in frequency) is set by the micro-cavity free-spectral range (FSR) F_a. Quantitively, the mth resonance $f_m^{(b)}$ of a super-mode can be linked to the micro-cavity resonances $f_m^{(a)}$ by the relation

$$f_m^{(b)} = f_m^{(a)} - (\Delta - q - m\,\delta)\,F_b, \qquad (1)$$

where F_b is the main-cavity FSR and q is an integer defining the order of the super-mode (see Fig. 1b). In general, the q-order super-mode is frequency detuned with respect to the micro-cavity resonance by $(\Delta - q)\,F_b$, where Δ is the cavity-frequency offset, normalised against F_b. The key features of the laser are determined by the leading-order super-mode, defined for $q = 0$, which possesses the largest spectral

overlap with the micro-cavity resonances. Higher-order super-modes ($q \neq 0$) typically experience greater coupling losses. Because F_b is not necessarily an integer divisor of F_a, we introduce the variable δ, normalised against F_b, representing the FSR detuning.

Two numerical examples of linear and solitary propagation are reported in Fig. 2. We use a spatial coordinate periodically closed over the micro-cavity length because the temporal waveform of every super-mode is periodic with the micro-cavity round-trip time T_a, with a period slightly detuned by δ (Eq. (1)). The parameters $\Delta - q$ and δ play the role of the frequency and group velocity mismatches between the micro-cavity and super-mode fields. A key property of solitary waves in vectorial equations, also recently shown for spatio-temporal mode-locking [29], is that all the coupled fields *lock* to a single group velocity (or repetition-rate detuning) v (Fig. 2a and b) and carrier frequency offset ϕ (Fig. 2c, see also model Equations in the Methods). Practically, the system provides a well-defined soliton comb, with the n^{th} frequency tooth $f_n^{(S)}$ expressed as

$$f_n^{(S)} = f_n^{(a)} + (\phi - n\, v)\, F_b. \tag{2}$$

The parameters ϕ and v are selected by Δ and δ, together with the normalised saturated gain g (Methods/Supplementary).

The measurements of laser cavity soliton micro-combs at different intra-cavity powers are in Fig. 3a-f. The spectra exhibit a bandwidth of up to 50 nm - comparable to the cavity-solitons observed in resonators with similar dispersion properties [9,20,21] - and, together with the corresponding autocorrelations (Fig. 3a, c, e and inset), are in excellent agreement with theory.

We used intra-cavity laser-scanning spectroscopy (see Methods) (Fig. 3b, c and f) to measure the frequency of the oscillating modes and their position within the micro-cavity resonance, obtaining important insights into the solitary nature of the solution.

A bistable system can display both localised and non-localised coherent waves [22]. Solitons are localised states that can appear in groups of non-equidistant pulses, such as the triplet seen in Fig. 3e-f. The stability of their tails requires the stability of the background, which is theoretically expected for oscillating modes that are red-detuned with respect to the micro-cavity resonance (Methods, Supplementary and Fig. 4a). These facts are in excellent agreement with the measurements shown in Figs. 3b, d and f. We attribute the small, blue-detuned mode found only in the central resonance to a perturbation on the soliton tails, against which localised pulses are robust (Supplementary).

Conversely, coherent patterns are non-localised, periodic waves which fill the entire cavity. Type I [2] and type II combs in the Lugiato-Lefever system are characteristic examples of patterns that typically have a narrower bandwidth than solitons. Earlier observations, [2,38-40] limited to picosecond pulse durations and displaying Type I ([39] and Supplementary) and II [40] comb shapes, are consistent with this picture. Furthermore, laser scanning spectroscopy measurements (see Supplementary and [40]) on these types of pulses reveal blue-detuned modes, for which the theory forbids stable solitons but while allowing patterns originating from the modulational instability of the background state [22].

Our experiments demonstrate the inherently higher efficiency of our class of laser cavity-solitons compared to Lugiato-Lefever solitons that feature a dominant comb mode, located at the pump wavelength, comprising the energy of the CW background (Fig. 4b-c). For Lugiato-Lefever solitons, the mode efficiency has a theoretical limit of 5% and 50% for bright and dark solitons, respectively [23]. Our mode efficiency in the experiments of Fig. 3 is greater than 75% for bright solutions. Further, we theoretically predict a maximum mode efficiency of 96% for bright laser cavity-solitons. This contrasts with state-of-the-art devices based on bright Lugiato-Lefever solitons that have mode efficiencies on the order of 1.6% to 5% [23,31]. Lugiato-Lefever solitons feature a minimum power excitation threshold

above which the Kerr nonlinearity induces bistability, yielding the two CW states necessary for the soliton's existence (Fig.4a). Our laser cavity-solitons, in contrast, require a zero background with a single CW state and exist below the Kerr bistability threshold. By comparing experiment with theory, we find that our peak powers injected into the micro-cavity are below 50% of the input power *threshold* of a Lugiato-Lefever soliton for the same micro-resonator. Because our injected field is pulsed, the injected average power to the micro-resonator is less than 6% of this threshold power (Supplementary).

To demonstrate the capability of changing the soliton repetition-rate using simple methods, we varied the main-cavity FSR detuning δ with a delay line that modified the fibre cavity length, and hence the mode-spacing F_b. Gain and loss were also adjusted to maintain the solitary state. Fig. 5 shows the repetition-rate variations for three cases (Fig. 5a). We measured the frequency position of the comb modes against the mode number using laser-spectroscopy. We then calculated the best-fit for the first case (Comb 1) and subtracted the frequency positions for the three cases, obtaining the residual frequency versus mode number in Fig. 5b. This shows a change in repetition-rate of over a megahertz. The theoretical results (Fig.5c and Supplementary) demonstrate that, by changing δ within the experimentally achievable range, the soliton stability is maintained while its velocity is modified – thus varying the repetition rate.

Finally, we achieve these localised states by manual adjustment of the fibre cavity parameters, such as cavity length, gain current and polarisation losses, in a similar fashion to passively mode-locked lasers. This approach enables the use of powerful methods, such as genetic algorithms, that have been instrumental in achieving adaptive control of the soliton properties and self-starting operation in passive mode-locking [41].

In conclusion, we report the observation of temporal laser cavity-solitons in optical micro-combs. Our results merge the powerful physics of optical Kerr micro-combs and their ability to generate large bandwidths with the unique properties of laser cavity-solitons and multi-mode systems. In contrast to conventional coherently-driven cavity-solitons, this new class of cavity-solitons is intrinsically background free, making them extremely energy efficient. Furthermore, thanks to a tailored two-cavity configuration, crucial properties, such as the repetition-rate, can be controlled with simple elements such as a delay line. Laser-cavity solitons represent a new and powerful mode of operation for micro-combs, offering many advantages that will help pave the road towards enabling these devices to move out of the laboratory towards real-world applications.

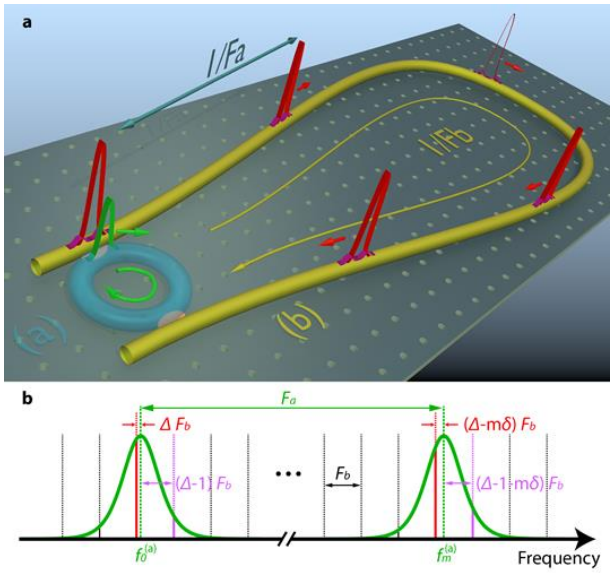

Figure 1. Principle of operation of micro-comb laser cavity-soliton formation. **a.** A short pulse (green) propagates in the micro-cavity (blue) sustained by a longer pulse (red) and a weak higher-order 'super-mode pulse' (purple) in the amplifying loop (yellow). This depicts the fundamental operation of a single soliton per cavity. **b.** Cold-cavity spectral distribution. Micro-cavity resonances are depicted in green, amplifying-cavity resonances are in black, with leading and first-order super-modes highlighted in red and purple, respectively. The normalised frequency offset between the central frequency of the leading super-mode and the micro-cavity resonance is Δ; similarly, the frequency offset is Δ-1 for the central frequency of first-order super-mode. In the convention used here and in Eq. (1), positive values of Δ correspond to a leading order super-mode red-detuned with respect to the micro-cavity resonances. The variable δ is the normalised FSR detuning, appearing when the two cavities are not commensurate.

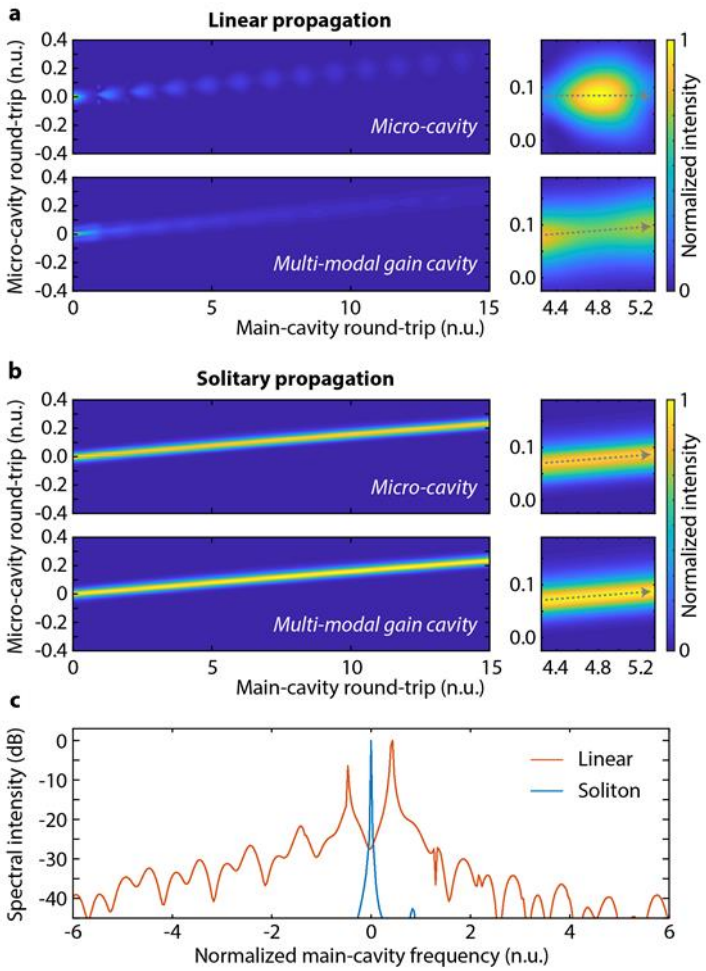

Figure 2. Theoretical propagation of linear and solitary pulses. Micro-cavity and gain cavity have a group velocity mismatch δ = 0.03. In these examples we used Δ =0.47; g= 0.14 and N=30 in Eqs. (3) and (4) in the Methods. **a.** Evolution of the micro-cavity and multi-modal amplifying-cavity fields in the linear case. The quantities in the upper and lower panels are the overall field intensities in the two cavities are $|a(t,x)|^2$ and $\sum_{-N}^{N}|b_q(t,x)|^2$, with reference to Eq. (3) and (4) in the Methods. The group velocity of the fields is better shown in the insets, where the direction of the field is marked with an arrow. The mismatch between such group velocities causes a periodical decoupling of the fields. **b.** Solitary propagation: both fields lock to the same group velocity v. **c.** Equivalent spectral distribution of the super-modes within a resonance of the micro-cavity (Supplementary). Such a spectrum, for the linear case (orange), highlights the presence of many frequency components, one for every super-mode with frequency offset $\Delta - q$. In the case of solitary propagation (blue), conversely, all the modes *lock* to the frequency ϕ.

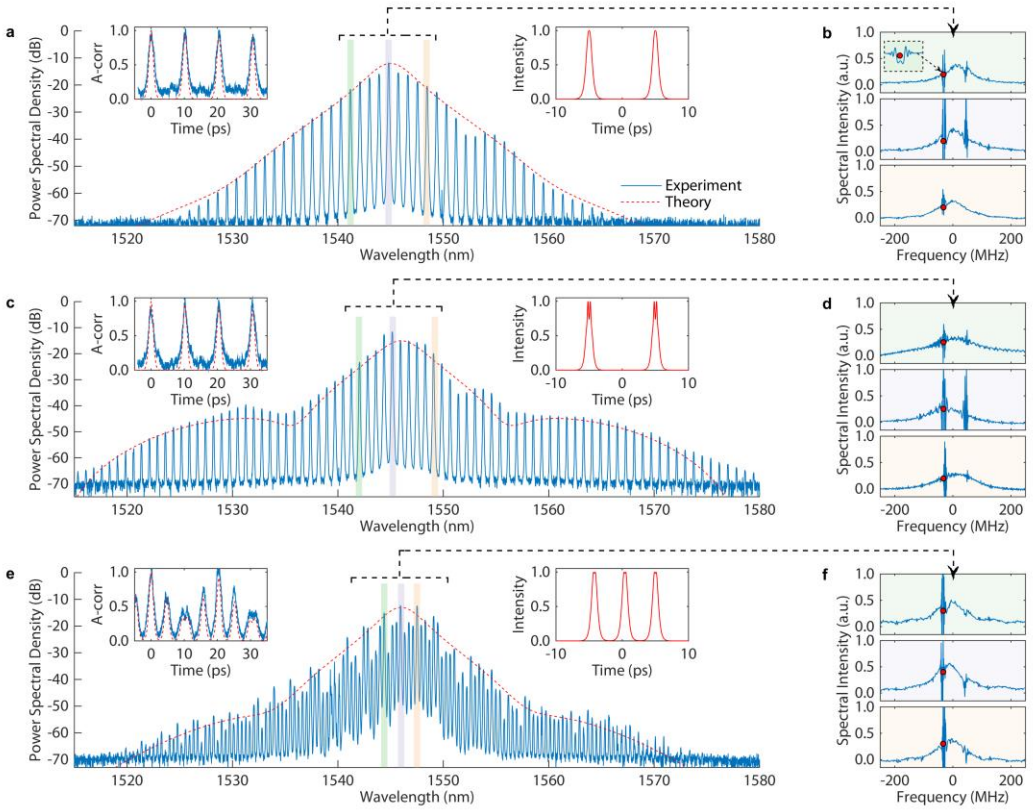

Figure 3. Temporal laser cavity-soliton measurement. a. Soliton generation, for two equidistant solitons per round-trip. Intra-cavity power at the output of the amplifier is 100 mW and at the output of the micro-cavity is 20 mW. Spectrum (in logarithmic scale) and autocorrelation (left inset). The experimental measurements (blue) are compared to the theoretical solitary state (red). Fit parameters are Δ = 0.49; g= 0.1. The theoretical normalised soliton frequency is $\phi = -0.475$, corresponding to a red-shifted frequency of 36 MHz (Eq. 2) for F_b = 77 MHz (Methods). The right inset reports the theoretical intensity profile in the micro-cavity. **b.** Intra-cavity spectrum (blue), evidencing within each micro-cavity resonance the lasing modes (red dots, red-shifted of approximately 32 MHz from the micro-cavity centre, in excellent agreement with the theory). The three plots correspond to the comb wavelengths highlighted in panel (a) by different colour shading. **c, d.** The same measurements at higher fibre gain for two equidistant solitons per round-trip, leading to 150 mW intra-cavity power at the output of the amplifier and 30 mW at the output of the ring, showing that the bandwidth of the soliton increases with the gain. Fit parameters are Δ =0.47; g= 0.14, with $\phi = -0.474$. The shape of the spectrum diverges from the sech-like, triangular shape of the case a,b. The formation of the lateral wings can be qualitatively related to a modulational instability effect on the peak of the pulse, shown in the theoretical intensity pulses in the right inset [22]. **e, f.** The same measurements for three solitons per round-trip for the same intra-cavity power of case c, d. Fit parameters are Δ = 0.49; g = 0.11, with $\phi = -0.477$. Because there is an additional soliton in the cavity, the energy per soliton is lower than the case c,d, leading to a narrower spectrum. The autocorrelation shows that the solitons are not equidistant, highlighting the localised nature of the solution.

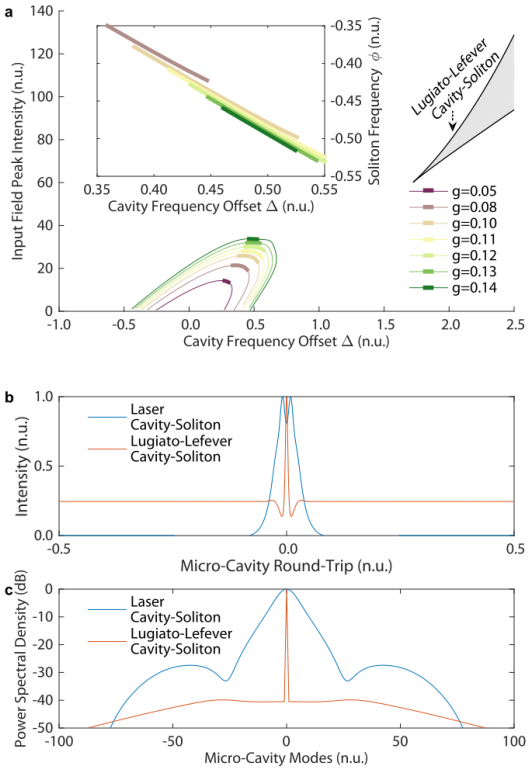

Figure 4. Temporal laser cavity-soliton and Lugiato-Lefever cavity-soliton comparison. a. Plot of laser cavity-soliton input field peak power versus normalised offset Δ, calculated for various gain values (g=0.05 to 0.14 for plots from purple to green). Thick lines mark the stable self-localised solutions, both in the main graph and the inset, where it is reported the soliton frequency ϕ. Note that negative values of ϕ correspond to red-shifted frequencies with respect to the micro-cavity centre, in agreement with the experiments. The grey region marks the region of existence of the Lugiato-Lefever bright solitons. **b.** Intensity profile in the micro-cavity for a laser cavity-soliton (Δ =0.47; g= 0.14, blue line) and a Lugiato-Lefever cavity-soliton at the power threshold (orange line), highlighting the presence of a strong background in the Lugiato-Lefever case. **c.** Spectrum of the theoretical cases in b. The strong background of the Lugiato-Lefever cavity soliton results in a dominant comb mode at the centre of the spectrum. Laser cavity-soliton line generally possess higher power spectral density.

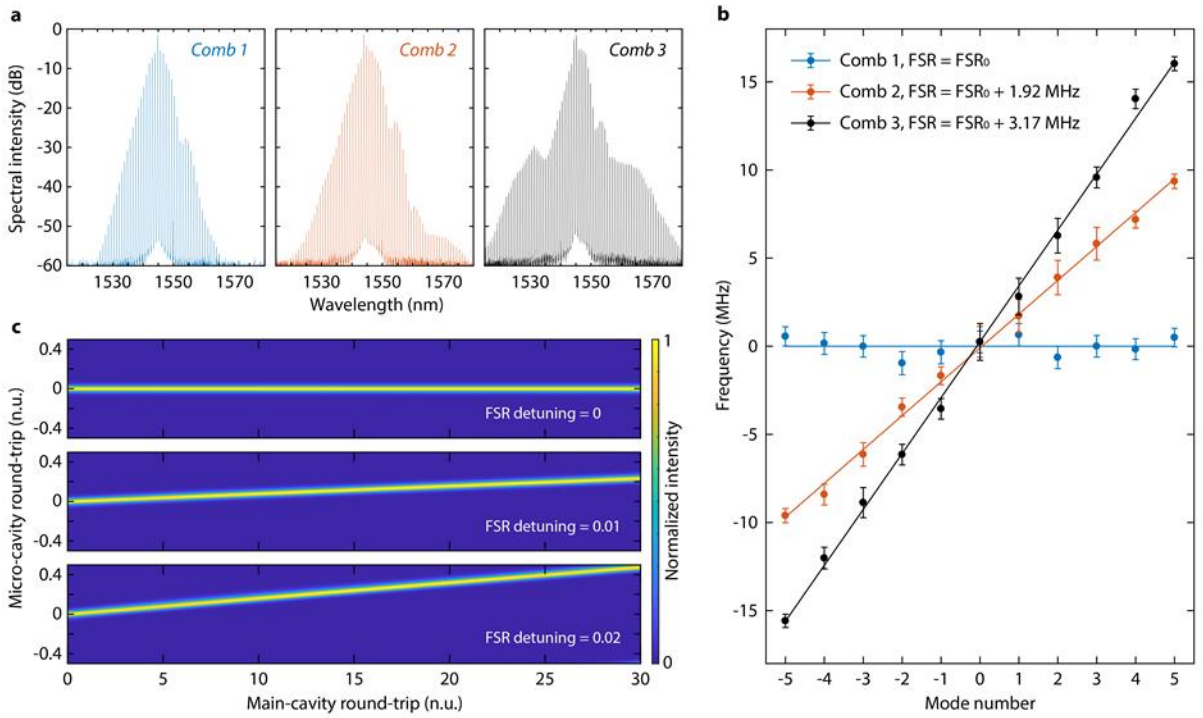

Figure 5. Temporal laser cavity-soliton repetition-rate control. a. Spectra. The fibre cavity length is changed within a broad range of 150 μm. Gain and losses had been readjusted to maintain the solitary state showing two equidistant solitons per round-trip; intra-cavity powers are 20 mW, 25 mW and 30 mW, in blue, orange and black, respectively. **b.** Residual frequency shift against mode number with respect to the best-fit for the Comb 1 case (blue). Combs 2 and 3 show a change in FSR and, hence, repetition-rate variations of 1.9MHz and 3.2MHz with respect to Comb 1. **c.** Calculated propagation of a stationary solitary solution when Δ =0.49 and g= 0.1, for $\delta = 0; 0.01; 0.02$. The solitary wave is maintained in all three cases.

Methods

Experimental Setup

The experimental setup is built around a high index doped silica integrated resonator with FSR~48.97 GHz and linewidth ΔF_A <140MHz (within the experimental measurement uncertainties), corresponding to a Q factor of ~1.3 million. The micro-resonator has a minimum in the transmission spectrum around 1552 nm, which is visible also in the comb generation and features transmission losses of 60%.

The micro-ring was inserted in an anomalous dispersion, polarisation-maintaining Ytterbium-Erbium co-doped fibre-cavity. This cavity comprised a delay line, polarisation optics, an optical isolator as well as a 10 nm tuneable bandpass filter (resulting, when matched to the amplifier spectral response, in a Gaussian linewidth of ΔF_F =650 GHz). Note that the soliton spectra in Fig. 3 and 4 well exceed such a bandwidth. The FSR of the cavity was about 77 MHz.

In sharp contrast to passively mode-locked lasers that intrinsically need a gain-dampening mechanism, cavity-solitons do not necessitate a fast-saturable absorption because they arise from the bistability of the system [22]. For this reason, we used a full polarisation-maintaining loop to prevent any effect related to fast gain saturation and standard passive mode-locking, further confirming the bistable origin of the pulses. Note that the fibre amplifier had a recovery time in the order of 10 ms [42], well above the soliton repetition-rate and main-cavity round-trip.

The intra-cavity lines were measured by laser-scanning spectroscopy (Supplementary). The scanning laser was calibrated with a 6.95 MHz Mach-Zehnder and by beating it with a 250MHz reference comb [43]. The micro-comb output was extracted at the drop-port of the micro-ring and was characterised with a second harmonic generation, background-free, non-collinear autocorrelator, optical spectrum-analyser and radio-frequency detection, obtained with a fast oscilloscope. The intra-cavity energy was measured with two monitors at the drop-port of the micro-resonator and the output of the amplifier before all system losses.

The soliton cases presented in the experiments show the presence of multiple pulses in the cavity. Our present setup could not run at a lower saturation powers which would allow for the observation of single soliton states.

Soliton states could be maintained over a time scale of minutes. The long-term stability of the solitary state was limited by mechanical and acoustical perturbations. Electronic feedback and proper packaging to screen mechanical and acoustical perturbations is expected to improve the system stability.

Model

The main features of the laser can be obtained by a simple mean-field model (see Supplementary for the complete derivation) that, in its normalised form, reads:

$$\partial_t a + \frac{i\zeta_a}{2}\partial_{xx}a + i\,|a|^2 a = -\kappa a + \sqrt{\kappa}\sum_{q=-N}^{N} b_q \quad (3)$$

$$\partial_t b_q + \delta\partial_\tau b_q + \frac{i\zeta_b}{2}\partial_{xx}b_q - 2\pi\, i\,(\Delta - q)b_q = \sigma\partial_{xx}b_q + g\, b_q - \sum_{p=-N}^{N} b_p + \sqrt{\kappa}a, \quad (4)$$

where a and b_q are the optical field envelopes for the micro-resonator and amplifying cavities, respectively, and are expressed as a function of the normalised propagation time t and space coordinate x.

Here we have considered the generic interaction with 2N+1 super-modes b_q, for $|q| \leq N$; the mode with $q=0$ corresponds to the leading mode.

The time t accounts for the propagation over different round-trips and is normalised against the main-cavity round-trip $T_b=1/F_b$=12.5 ns. The space coordinate x, defined for $|x|<1/2$, is associated to the frame moving with the pulse and is normalised against the micro-cavity round-trip length, which corresponds to a round-trip time $T_a=1/F_a$ =20 ps.

The left- and right-hand sides of the equations contain the conservative and dissipative terms: $\zeta_{(a,b)}>0$, Δ and δ are the normalised coefficients for the cavity (anomalous) dispersions, the cavity-frequency offset and the group velocity mismatch. The latter term considers the effective FSR detuning between the two cavities as in Eq. (1); κ, g and σ represent the coupling, saturated gain and bandwidth of the spectral-filtering, respectively.

Specifically (see Supplementary for the derivation), the normalised coupling parameter is $\kappa = \pi \Delta F_A T_b \approx 2\pi$, being the micro-cavity linewidth ΔF_A approximately twice the FSR of the main-cavity (in the experimental condition). The normalised dispersions are $\zeta_{(a,b)} = -\beta_{(a,b)} v_{(a,b)} T_b / T_a^2$ for which $v_{(a,b)}$ and $\beta_{(a,b)}$ are the group-velocities and group velocity dispersions of the two cavities, respectively. In the simulations, we used $\zeta_a = 1.25 \times 10^{-4}$, $\zeta_b = 3.5 \times 10^{-4}$, obtained with values $|\beta_a|$≈-20 ps²/km and $|\beta_b|$≈-60 ps²/km (within our experimental constraints). We used a gain bandwidth $\sigma = (2\pi T_a \Delta F_F)^{-2} \approx 1.5 \times 10^{-4}$, based on a 650 GHz intra-cavity spectral filter. The gain g, considered as the saturated-gain of the amplifier, is normalised against the main-cavity length and, together with Δ and δ in Eq. (1), is an adjustable parameter in our numerical datasets.

The stationary states are defined as $a(t,x) = a_S(x - vt) \exp[2\pi i \phi t]$, $b_q(t,x) = b_{q,S}(x - vt) \exp[2\pi i \phi t]$, where the normalised frequency offset ϕ and the normalised velocity v are as in Eq. (2). Solitary solutions are found by numerical continuation considering 11 super-modes (i.e. with N=5), while stability is investigated with linear perturbation analysis and propagation considering 61 super-modes (i.e. with N=30).

Acknowledgment

We acknowledge the support of the U.K. Quantum Technology Hub for Sensors and Metrology, EPSRC, under Grant EP/M013294/1 and from INNOVATE UK, project 'IOTA' grant agreement EP/R043566/1. A.P. acknowledges the support from the People Programme (Marie Curie Actions) of the European Union's FP7 Programme under REA grant agreement CHRONOS (327627). M.P. acknowledges the support by EU-H2020, research and innovation programme under REA grant agreement TIMING (725046) and from the People Programme (Marie Curie Actions) of the European Union's FP7 Programme under REA grant agreement THEIA (630833). B.W. acknowledges the support from the People Programme (Marie Curie Actions) of the European Union's FP7 Programme under REA grant agreement INCIPIT (PIOF-GA-2013-625466).

R.M. acknowledges funding by the Natural Sciences and Engineering Research Council of Canada (NSERC) through the Strategic, Discovery, and Acceleration Grants Schemes, by the MESI PSR-SIIRI Initiative in Quebec, by the Canada Research Chair Program, as well as additional support by the Government of the Russian Federation through the ITMO Fellowship and Professorship Program (grant 074-U 01) and by the 1000 Talents Sichuan Program.

Author Contributions

A.P., H.B. and M.P. developed the original concept. B.E.L. and S.T.C. designed and fabricated the integrated devices. H.B performed the experiments. A.P developed the theoretical model. A.C., M.R., L.D.L., J.S.T.G., G.-L.O., D.J.M., R.M. and B.W. contributed to the development of the experiment, numerical model and to the

data analysis. A.P., B.W., G.-L.O., D.J.M., R.M., H.B. and M.P. contributed to the writing of the manuscript. B.W., M.P., and A.P. supervised the research.

References

[1] Kippenberg, T. J., Holzwarth, R. & Diddams, S. A. Microresonator-based optical frequency combs. *Science* **332**, 555–559 (2011).

[2] Pasquazi, A. et al. Micro-combs: A novel generation of optical sources. *Phys. Rep.* **729**, 1-81 (2017).

[3] Suh, M.-G., Yang, Q.-F., Yang, K. Y., Yi, X. & Vahala, K. J. Microresonator soliton dual-comb spectroscopy. *Science* **354**, 600–603 (2016).

[4] Yu, M. et al. Silicon-chip-based mid-infrared dual-comb spectroscopy. *Nat. Commun.* **9**, 1869 (2018).

[5] Marin-Palomo, P. et al. Microresonator-based solitons for massively parallel coherent optical communications. *Nature* **546**, 274–279 (2017).

[6] Pfeifle, J. et al. Optimally Coherent Kerr Combs Generated with Crystalline Whispering Gallery Mode Resonators for Ultrahigh Capacity Fiber Communications. *Phys. Rev. Lett.* **114**, 093902 (2015).

[7] Liang, W., Eliyahu, D., Ilchenko, V. S., Savchenkov, A. A., Matsko, A. B., Seidel, D., & Maleki, L. High spectral purity Kerr frequency comb radio frequency photonic oscillator. *Nat. Commun.* **6**, 7957 (2015).

[8] Spencer, D. T. et al. An Optical-Frequency Synthesizer Using Integrated Photonics, *Nature* **557**, 81-85 (2018).

[9] Trocha, P. et al. Ultrafast optical ranging using microresonator soliton frequency combs. *Science* **359**, 887-891 (2018).

[10] Suh, M.-S. & Vahala, K. J. Soliton microcomb range measurement. *Science* **359**, 884-887 (2018).

[11] Kues, M. et al. On-chip generation of high-dimensional entangled quantum states and their coherent control. *Nature* **546**, 622–626 (2017).

[12] Reimer, C. et al. Generation of multiphoton entangled quantum states by means of integrated frequency combs. *Science* **351**, 1176-1180 (2016).

[13] Brasch, V. et al. Photonic chip–based optical frequency comb using soliton Cherenkov radiation. *Science* **351**, 357–360 (2016).

[14] Del'Haye, P. et al. Phase-coherent microwave-to-optical link with a self-referenced microcomb. *Nat. Photonics* **10**, 516-520 (2016).

[15] Suh, M.-G. et al. Searching for exoplanets using a microresonator astrocomb. *Nat. Photonics* 13, 25-30 (2019).

[16] Obrzud, E. et al. A microphotonic astrocomb. *Nat. Photonics* 13, 31-35 (2019).

[17] Haelterman, M., Trillo, S. & Wabnitz, S. Dissipative modulation instability in a nonlinear dispersive ring cavity. *Opt. Commun.* **91**, 401-407 (1992).

[18] Leo, F. et al. Temporal cavity-solitons in one-dimensional Kerr media as bits in an all-optical buffer. *Nat. Photonics* **4**, 471–476 (2010).

[19] Herr, T. et al. Temporal solitons in optical microresonators. *Nat. Photonics* 8, 145–152 (2013).

[20] Xue, X. et al. Mode-locked dark pulse Kerr combs in normal-dispersion microresonators. *Nat. Photonics* **9**, 594–600 (2015).

[21] Cole, D. C., Lamb, E. S., Del'Haye, P., Diddams, S. A. & Papp, S. B. Soliton crystals in Kerr resonators. *Nat. Photonics* **11**, 671–676 (2017).

[22] Lugiato, L. A., Prati, F. & Brambilla, M. Nonlinear Optical Systems. (Cambridge University Press, 2015).

[23] Xue, X., Wang, P.-H., Xuan, Y., Qi, M. & Weiner, A. M. Microresonator Kerr frequency combs with high conversion efficiency. *Laser Photonics Rev.* **11**, 1600276 (2017).

[24] Yao, B. et al. Gate-tunable frequency combs in graphene–nitride microresonators. *Nature* **558**, 410-414 (2018).

[25] Tanguy, Y., Ackemann, T., Firth, W. J. & Jäger, R. Realization of a Semiconductor-Based Cavity Soliton Laser. *Phys. Rev. Lett.* **100**, 013907 (2008).

[26] Barland, S. et al. Cavity-solitons as pixels in semiconductor microcavities. *Nature* **419**, 699–702 (2002).

[27] Genevet, P., Barland, S., Giudici, M. & Tredicce, J.R. Cavity Soliton Laser based on Mutually Coupled Semiconductor Microresonators. *Phys. Rev. Lett.* **101**, 123905 (2008).

[28] Marconi, M., Javaloyes, J., Balle, S. & Giudici, M. How Lasing Localized Structures Evolve out of Passive Mode Locking. *Phys. Rev. Lett.* **112**, 223901 (2014).

[29] Wright, L. G., Christodoulides, D. N. & Wise, F. W. Spatio-temporal mode-locking in multimode fiber lasers. *Science* **358**, 94–97 (2017).

[30] Grelu, P. & Akhmediev, N. Dissipative solitons for mode-locked lasers. *Nat. Photonics* **6**, 84–92 (2012).

[31] Stern B., Ji X., Okawachi Y., Gaeta A.L., Lipson M. Battery-operated integrated frequency comb generator. *Nature* **562**, (7727), 401 (2018).

[32] Obrzud, E., Lecomte, S. & Herr, T. Temporal solitons in microresonators driven by optical pulses. *Nat. Photonics* **11**, 600–607 (2017).

[33] Yang, Q.-F., Yi, X., Yang, K. Y. & Vahala, K. Counter-propagating solitons in microresonators. *Nat. Photonics* **11**, 560–564 (2017).

[34] Miller, S. A. et al. Tunable frequency combs based on dual microring resonators, *Opt. Express* **23**, 21527–21540 (2015).

[35] Gustave, F. et al. Observation of Mode-Locked Spatial Laser Solitons. *Phys. Rev. Lett.* **118**, 044102 (2017).

[36] Krupa, K. et al. Spatial beam self-cleaning in multimode fibres. *Nat. Photonics* **11**, 237–241 (2017).

[37] Scroggie, A.J., Firth, W.J. & Oppo, G.-L. Cavity-soliton laser with frequency selective feedback, *Phys. Rev. A* **80**, 013829 (2009).

[38] Peccianti, M. et al. Demonstration of a stable ultrafast laser based on a nonlinear microcavity. *Nat. Commun.* **3**, 765 (2012).

[39] Wang, W. et al. Repetition rate Multiplication Pulsed Laser Source Based on a Microring Resonator. *ACS Photon.* **4**, 1677–1683 (2017).

[40] Bao H., Cooper A., Chu S.T., Moss D.J., Morandotti R., Little B.E., Peccianti M., Pasquazi A. Type-II Micro-comb generation in a filter-driven four wave mixing laser. *Photonics Research Journal* **6**, (5) B67-B73 (2018).

[41] Andral, U., Si Fodil, R., Amrani, F., Billard, F., Hertz, E. & Grelu, Ph. Fiber laser mode locked through an evolutionary algorithm. *Optica* **2**, 275-278 (2015).

[42] Haboucha, A., Leblond, H., Salhi, M., Komarov, A. & Sanchez, F. Analysis of soliton pattern formation in passively mode-locked fiber lasers. *Phys. Rev. A* **78**, 043806 (2008).

[43] Del'Haye, P., Arcizet, O., Gorodetsky, M. L., Holzwarth, R. & Kippenberg, T. J. Frequency comb assisted diode laser spectroscopy for measurement of microcavity dispersion. *Nat. Photonics* **3**, 529–533 (2009).